Interpretation of F-106B In-Flight Lightning Signatures

by
T. F. Trost
M. G. Grothaus
C. T. Wen

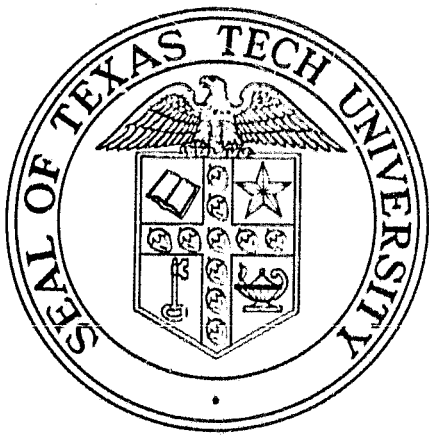

Report on N.A.S.A. Grant NAG-1-28

August 1985

(NASA-CR-176387) INTERPRETATION OF F-106B IN-FLIGHT LIGHTNING SIGNATURES (Texas Technological Univ.) 51 p HC A04/MF A01 CSCL 01C

N86-13320

Unclas
G3/05 04914

Department of Electrical Engineering/Computer Science
Texas Tech University
Lubbock, Texas 79409

INTERPRETATION OF

F-106B IN-FLIGHT LIGHTNING SIGNATURES

by

T. F. Trost
M. G. Grothaus
C.-T. Wen

Department of Electrical Engineering/Computer Science
Texas Tech University
Lubbock, Texas 79409

August, 1985

Prepared for

National Aeronautics and Space Administration
Langley Research Center
Hampton, Virginia 23665

Under Grant No. NAG-1-28
"Lightning Sensors and Data Interpretation"

ABSTRACT

This report consists of a series of short discussions covering various characteristics of the electromagnetic data obtained on a NASA F-106B aircraft during direct lightning strikes. Time scales of interest range from 10 ns to 400 μs. The following topics are discussed:

Lightning current, I, measured directly versus I obtained from computer integration of measured I-dot.

A method of compensation for the low-frequency cutoff of the current transformer used to measure I.

Properties of fast pulses observed in the lightning time-derivative waveforms.

The characteristic D-dot signature of the F-106B aircraft.

An RC-discharge interpretation for some lightning waveforms.

A method for inferring the locations of lightning channel attachment points on the aircraft by using B-dot data.

Simple, approximate relationships between D-dot and I-dot and between B and I.

Estimates of energy, charge, voltage, and resistance for a particular lightning event.

ACKNOWLEDGMENTS

The authors wish to thank M. E. Thomas of NASA Langley Research Center for supplying the digitized data used in this work and for providing much supporting information concerning the instrumentation of the F-106B aircraft.

TABLE OF CONTENTS

I. INTRODUCTION

During the past few years, lightning strikes to the NASA F-106B aircraft have yielded much new electromagnetic data on aircraft-lightning interactions. This report briefly examines several of the more obvious characteristics of the data. Results of controlled laboratory tests at Texas Tech University as well as results from approximate theoretical relationships are used for data interpretation. Most of the lightning strikes under discussion are from 1982, with just a single, although important, strike from 1984.

Related research activities at Texas Tech which are not explicitly discussed in the present work include an experimental study of the electromagnetic resonances of a model of the F-106B attached to resistive wires [1] and an experimental study of spark initiation on an isolated, conducting object in a strong electrostatic field (in progress).

II. RESULTS FROM 1982 DATA

Comparison of I and I-dot Sensors

Two transient recorders were used in 1982 and were switched among the four electromagnetic sensors shown in Fig. 1. A few lightning strikes were obtained with the recorders connected to the I and I-dot sensors, which measure the current and the time derivative of the current on the noseboom. The results from the strike which produced the largest current (82-44-04) are shown in Fig. 2. The lightning waveform depicted in the figure is a current pulse with a fast rise time and a slow fall time. The figure compares I to the time integral of I-dot in order to test the consistency of the two measurements. A small displacement in time has been introduced so that the two curves are not confused. Notice that the agreement overall is quite good. However, the effects of the coarse quantization of the 6-bit transient recorders are very evident: in the I waveform, the jumps between adjacent amplitude levels are quite large, and in the integrated I-dot waveform the entire trailing edge of the lightning pulse is represented by a constant slope. This constant decline resulted from a constant negative level in I-dot. The actual I-dot values were so small on the trailing edge of the pulse that the recorder digitized all of them in its first level below zero. This may be seen in the I-dot record, which is shown in Fig. 3. Refering to Fig. 3, notice also that the I-dot signal went off scale briefly during the fastest-rising portion on the leading edge of the pulse. Thus some positive area was missed for the integration. This is consistent with the fact that the integrated I-dot curve

LOCATIONS OF ELECTROMAGNETIC SENSORS ON F-106B AIRCRAFT

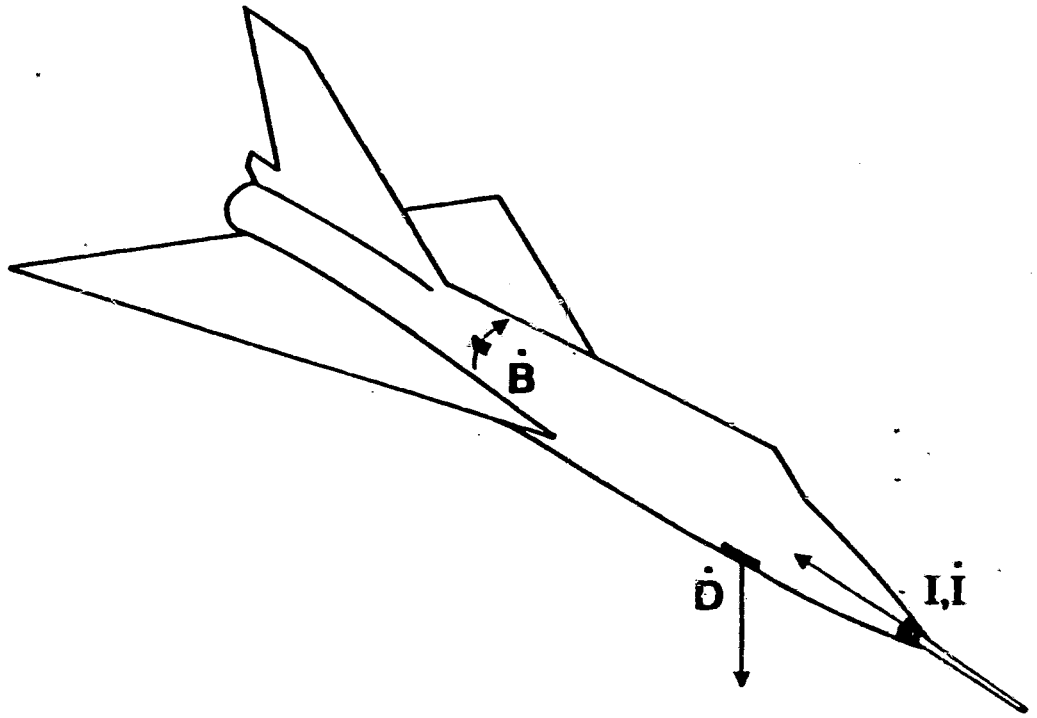

Fig. 1. Sensor locations for 1982. Arrows give the directions for which the various quantities (B-dot, D-dot, I, I-dot) are defined to be positive.

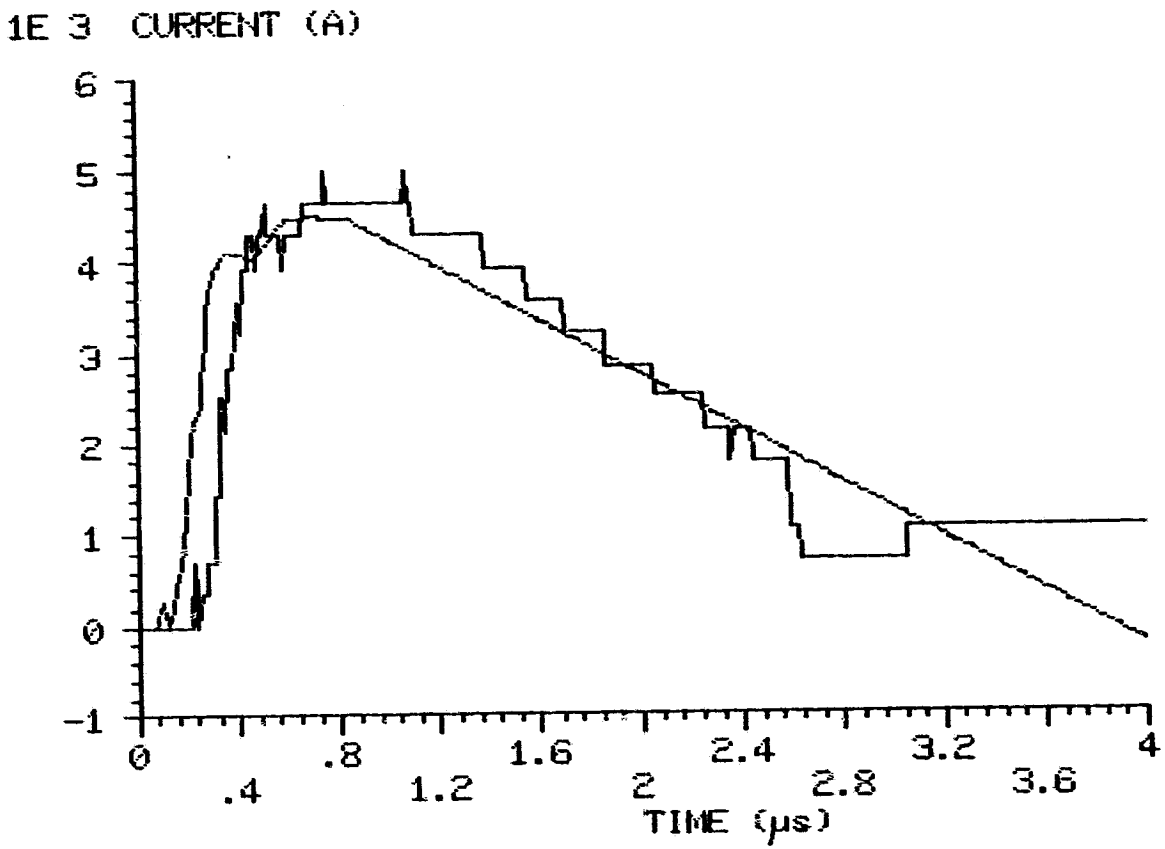

Fig. 2. Data comparison for strike 82-44-04. Smooth curve: time integral of I-dot waveform from I-dot sensor. Jagged curve: I waveform from current transformer.

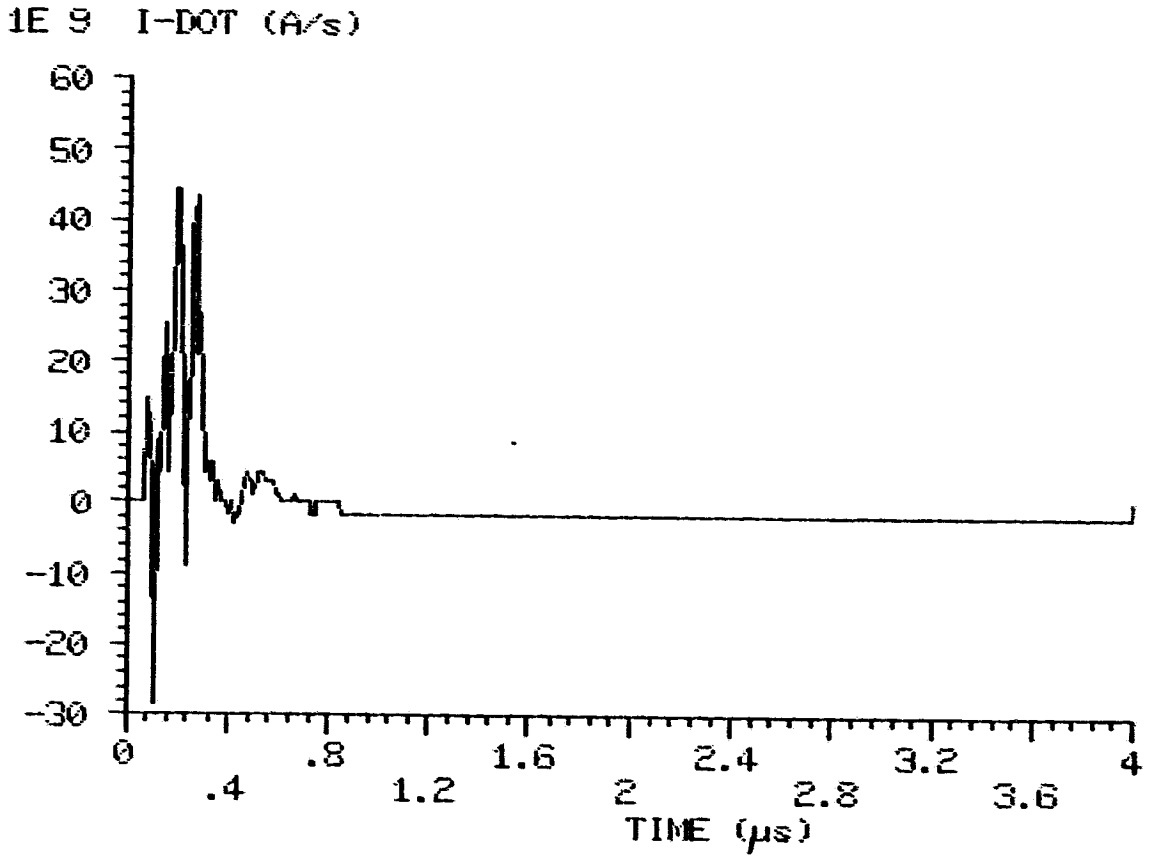

Fig. 3. I-dot waveform used to generate smooth curve in Fig. 2 (82-44-04).

in Fig. 2 goes slightly below the zero axis at the very end of the pulse.

I-Sensor Droop

For lightning signatures which varied more slowly than the pulse shown in Fig. 2, the I sensor was found to introduce distortion in the form of droop . This is to be expected since the I sensor was a current transformer with a lower cutoff (- 3 dB) frequency f_o = 2.8 kHz. Because of the droop, unipolar lightning currents appeared as bipolar at the sensor output, the effect being pronounced unless the lightning pulse lengths were much less than $(2\pi f_o)^{-1} \approx 60$ μs.

In order to estimate the true lightning signatures from the sensor output waveforms, we have measured the transfer function of the sensor in our laboratory and have written a computer program which uses the transfer function to put the low-frequency content back into the waveforms [2]. The program essentially just Fourier transforms the sensor output waveforms, divides by the transfer function, and inverse transforms the results. Two examples of waveforms processed with this program are shown in Figs. 4 and 5 (82-41-19 and 82-41-22). Each example shows the processed and unprocessed waveforms superimposed. Notice that most of the undershoot is removed by the processing and so is not a true characteristic of the lightning.

Fast Pulses in the Time-Derivative Waveforms

A common feature of many of the lightning time-derivative

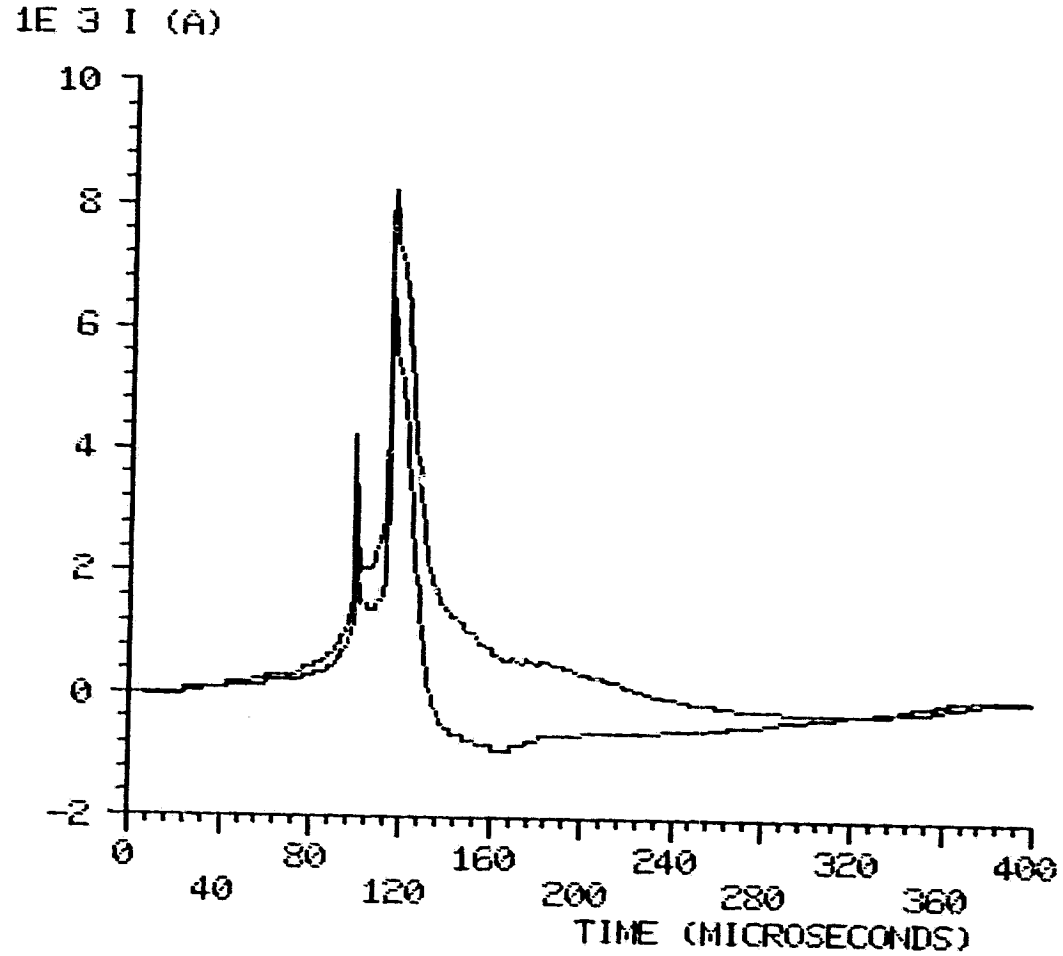

Fig. 4. Lightning current (I) waveform from current transformer, strike 82-41-19. Upper curve: processed. Lower curve: unprocessed.

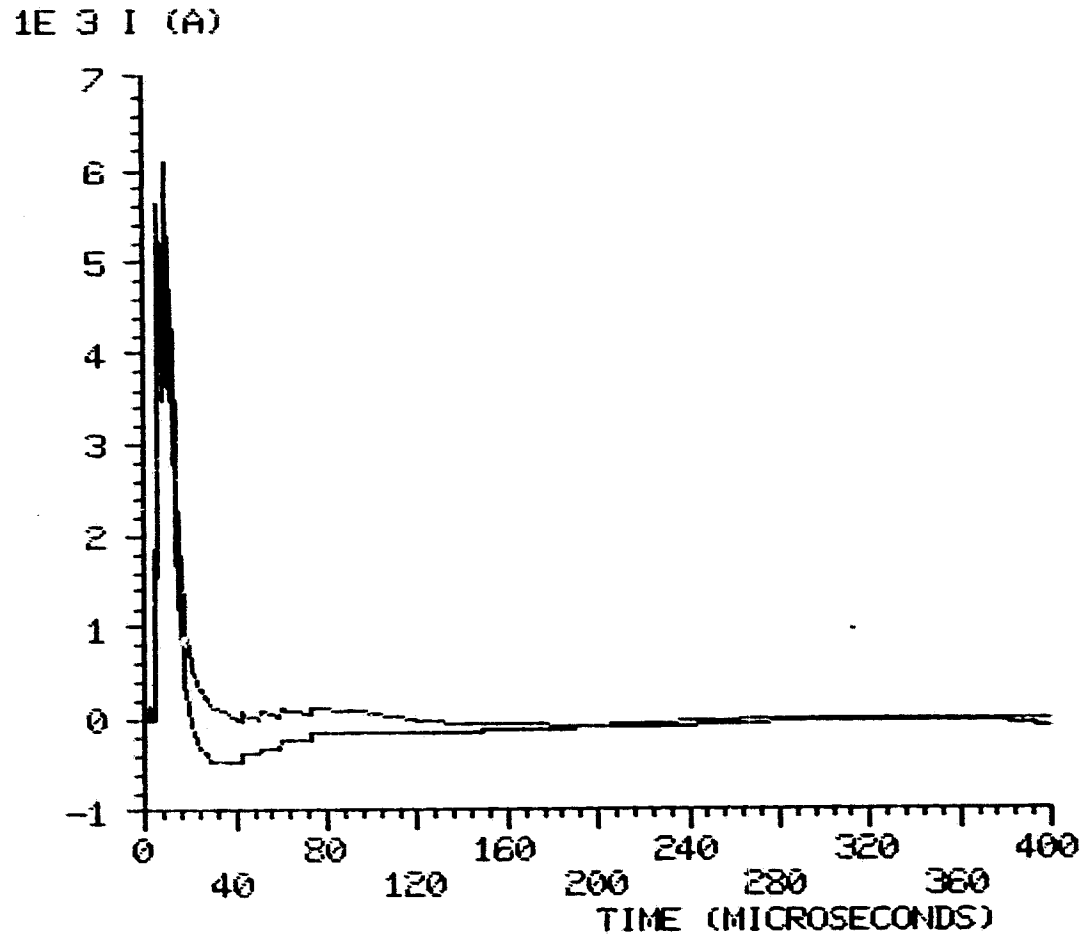

Fig. 5. Lightning current (I) waveform from current transformer, strike 82-41-22. Upper curve: processed. Lower curve: unprocessed.

waveforms is the appearance of very fast pulses. The pulses occur either singly or in groups, and the average number of pulses per group for 1982 was 2.4. An example of a group of 3 pulses in a D-dot waveform is shown in Fig. 6 (82-38-02). The 10 ns sample interval of the transient recorders is not short enough to provide detailed pulse shapes. In fact, the pulses are only two or three samples in width, and their true peak values are probably often missed in the sampling process. In 1982, surprisingly, all of the D-dot and B-dot pulses were of positive polarity. This corresponds to increasing positive charge at the front of the aircraft (where the D-dot sensor is located) and increasing current fore-to-aft along the fuselage (where the B-dot sensor is located). The fact that all the pulses had the same polarity implies a charging mechanism attached to the airplane. That is, an explanation for the charge accumulation based solely on the polarization of the airplane by an ambient electric field is not satisfactory since the ambient field would not always be oriented so as to put the same polarity of charge on the nose.

For the pulses that occurred in groups of two or more we have measured the time intervals between adjacent pulses. Fig.7 shows the distribution of these time intervals; the average value is 300 ns. Unfortunately, there is probably some inaccuracy in the distribution at short times because of the ringing of the aircraft. The pulses excite the electromagnetic resonances of the aircraft, which take about 300 ns to ring down [3]. (The period of the lowest-frequency resonance is about 160 ns.) Thus a weak pulse following within 300 ns of a strong one may be obscured by

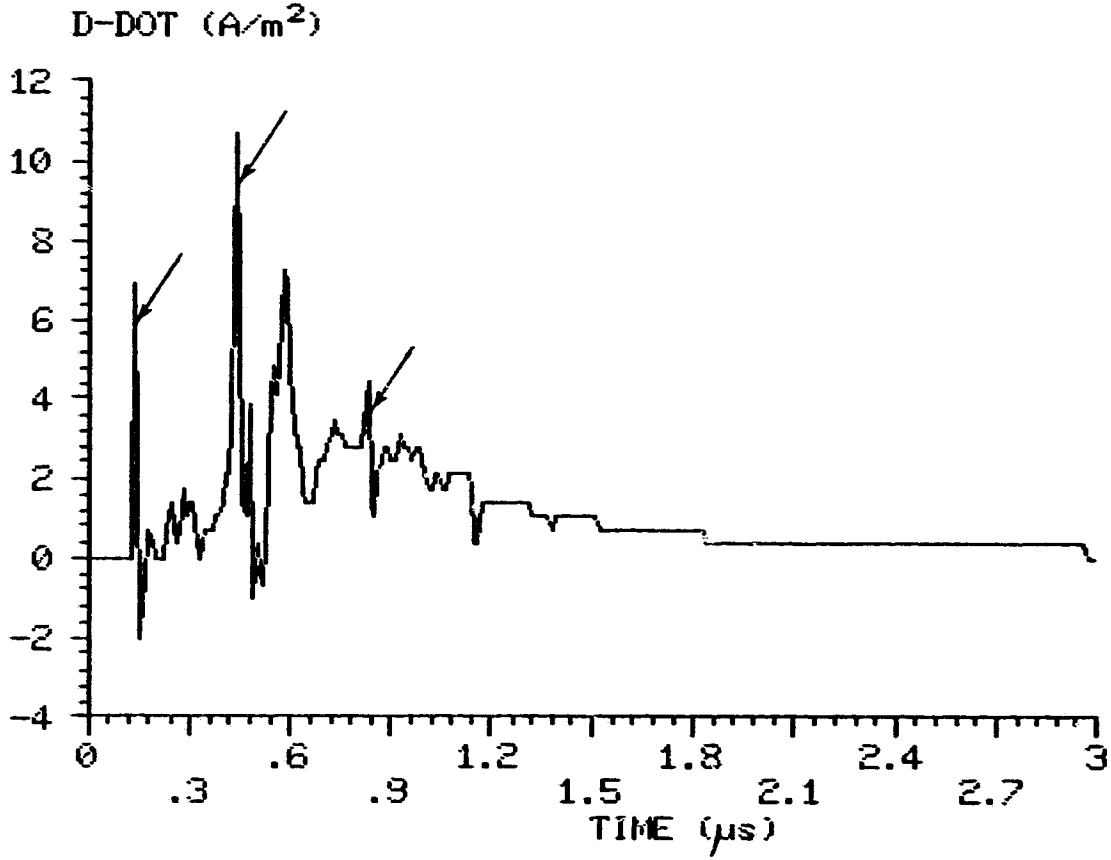

Fig. 6. D-dot waveform showing three fast pulses, strike 82-38-02.

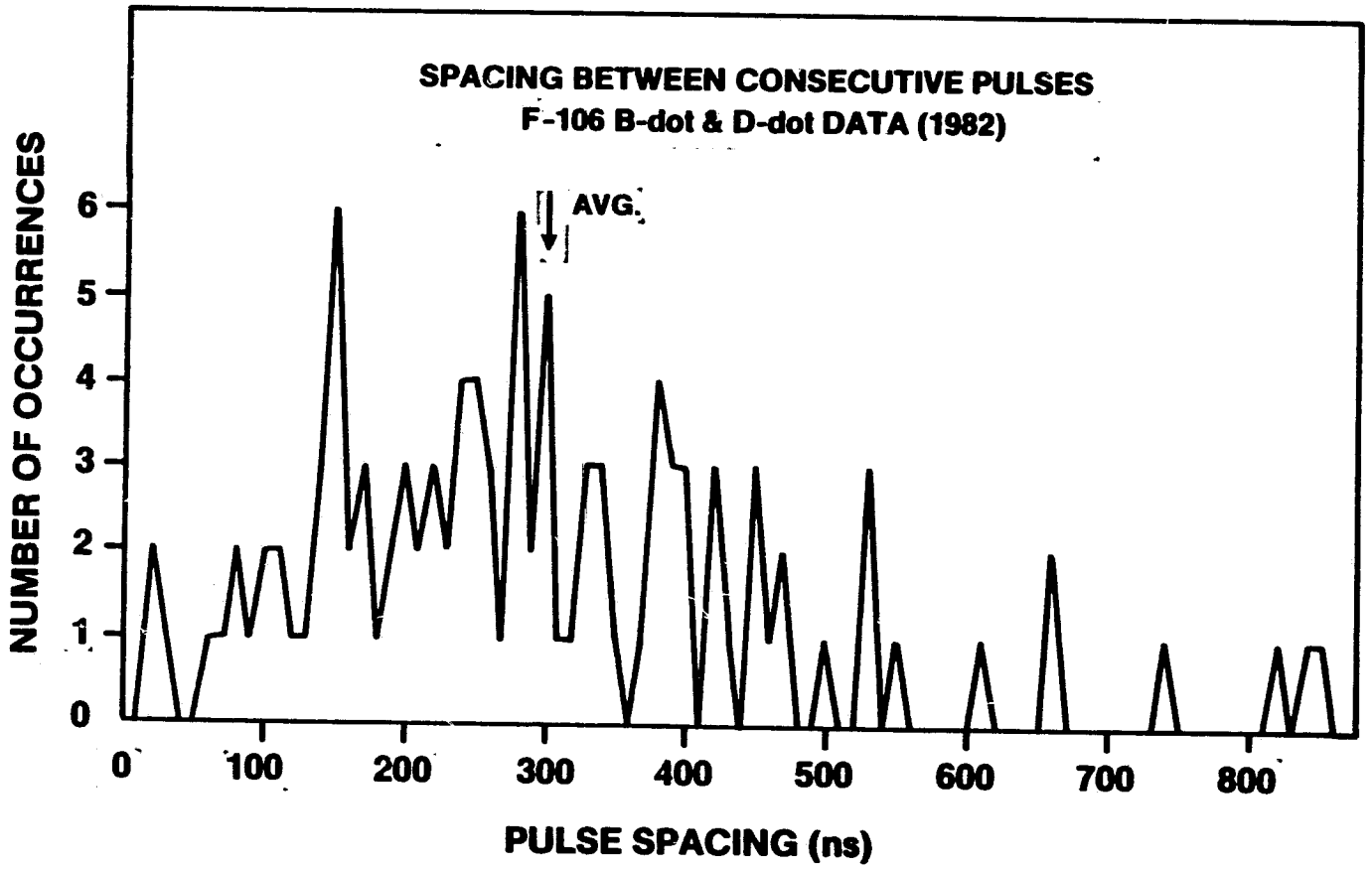

Fig. 7. Distribution of time spacing between consecutive pulses.

the ringing.

F-106B Signature

A typical example of aircraft ringing is seen in Fig. 6 following the second, and largest, pulse. An expanded plot of this portion of the waveform is shown in Fig. 8, labelled F-106. Notice that the ringing consists in part of a prominent double hump shape. This shape has also been observed in laboratory scale-model tests [4], and one of the waveforms from the laboratory model is shown in Fig. 8 for comparison with the F-106 data. From the laboratory tests it has been found that the double hump results from the reflection from the rear of the aircraft of a fast current change. That is, the shape is produced by a current step which is injected at the front of the aircraft, travels to the rear, and then partially reflects from the trailing edge of the wings (first hump) and then from the end of the fuselage and tail (second hump). This shape is a characteristic signature of the F-106 in response to current injection at the nose. It is clearly observed 58 times in the 1982 D-dot data.

The positive polarity of the pulse preceding the humps means a positive change in the charge on the nose, so that electrons must have exited there. See Fig. 9. This is an interesting result because it means that the nose of the aircraft was acting as a negative tip, and it is known from laboratory studies [5] that in a rod-plane gap, if the rod is negative, a higher voltage must be applied to cause sparkover than if the rod is positive.

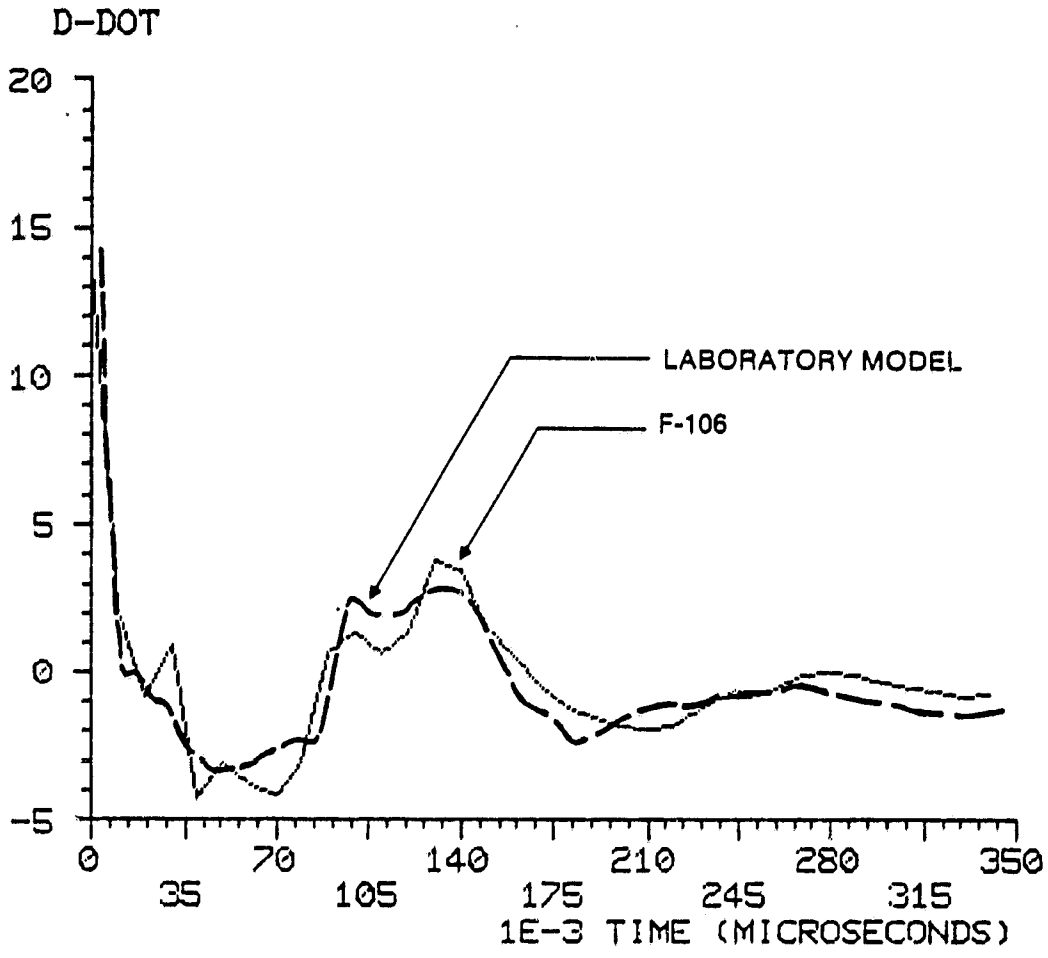

Fig. 8. Comparison of D-dot double hump signature of F-106B (82-38-02) and laboratory model.

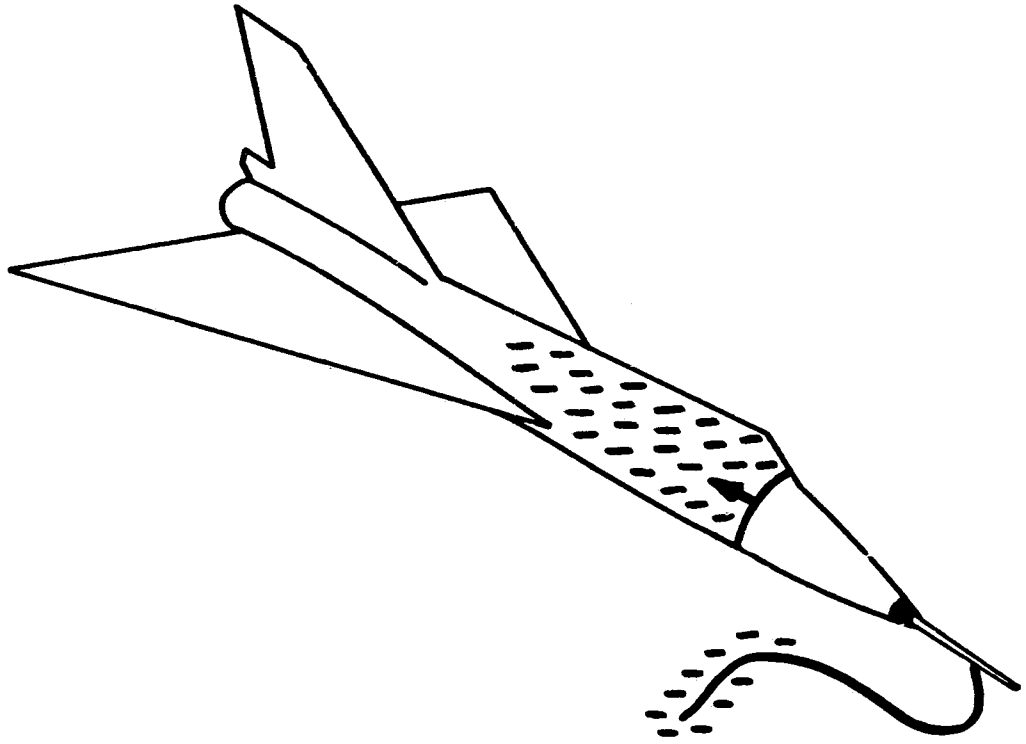

Fig. 9. Channel attachment to noseboom, and abrupt loss of electrons at nose which propagates aft.

Aircraft Discharging

The variation of electric field, E, corresponding to the D-dot waveform in Fig. 6 has been obtained by integrating and dividing by ϵ_0. The result is shown in Fig. 10. The fast pulses in D-dot appear as small, abrupt increases in electric field, while the main feature of E is an approximately exponential rise to 360 kV/m. This indicates that the aircraft experienced an increase in positive charge or a decrease in negative charge, with a time constant of about 680 ns. The location of the zero electric-field level is not known and has been arbitrarily located at the bottom of the plot. Three curves, rather than one, have been plotted in order to show the effect on E of the uncertainty in the exact value of D-dot due to the 6-bit quantization of the transient recorder. The middle curve is the integral of the actual D-dot data, and the upper and lower curves are, respectively, the integrals of the data after the D-dot zero level had been shifted up and down by 1/2 of a least-significant-bit (LSB).

Values of maximum E and time constant, τ, for several lightning strikes which showed approximately exponential discharging (or charging) like that in Fig. 10 are given in Table I. All of these waveforms were similar to Fig. 10 in that they contained, first, a brief slowly rising portion, then a few rapid increases, and finally a longer, quasi-exponential rise. The τ values were measured as the time required for the curves to reach $(1 - e^{-1})$ of their final value, not including the slow rise at the beginning.

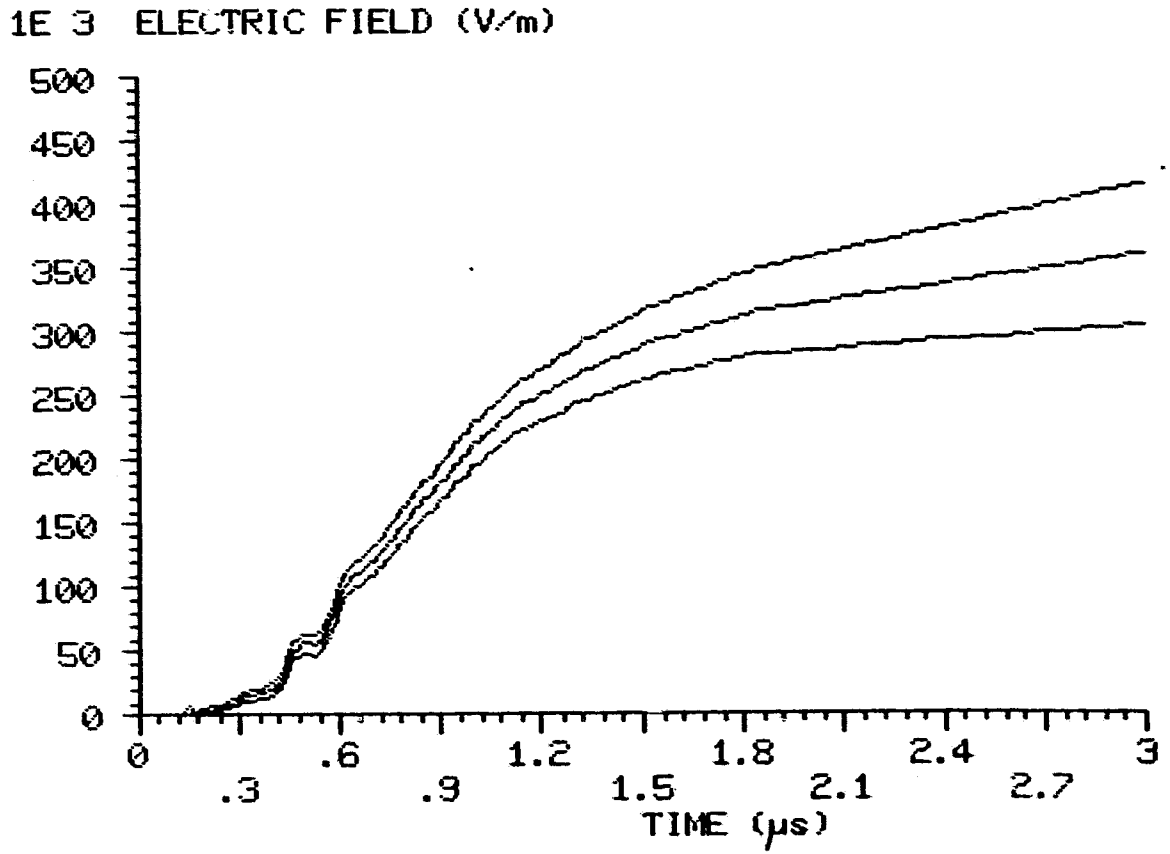

Fig. 10. E waveforms from time integral of D-dot in Fig. 6 (82-38-02).

Table I. Aircraft Discharging Parameters

Strike	Max. E (kV/m)	τ (ns)
82-38-02	360	680
82-38-04	120	670
82-40-04	190	500
82-40-07	440	370
82-42-06	160	630
82-42-09	240	600

Fig. 11 shows the waveform of B-dot that was recorded simultaneously with the D-dot waveform of Fig. 6. The time integral of B-dot is shown in Fig. 12, with the effect of a ± 1/2 LSB change in B-dot illustrated by the multiple curves. Unfortunately, these 1/2-bit changes cause a large variation in the final value of B, indicating the need for finer quantization. Actually, the B-dot waveform was altered in one respect prior to integration: the value of the large positive peak, which was at full scale for the recorder, was increased. If this had not been done, the final values of all three of the curves in Fig. 11 would have been negative, indicating a large continuing current flowing on the aircraft instead of a short pulse. While continuing current is possible, data recorded in 1984 suggest that the current in the present case was actually in the form of a short pulse. A quick look at 1984 data (84-17-01) shows D-dot and B-dot waveforms similar to those here, but in addition, thanks to an increase in the number of data channels, it also shows I; and the

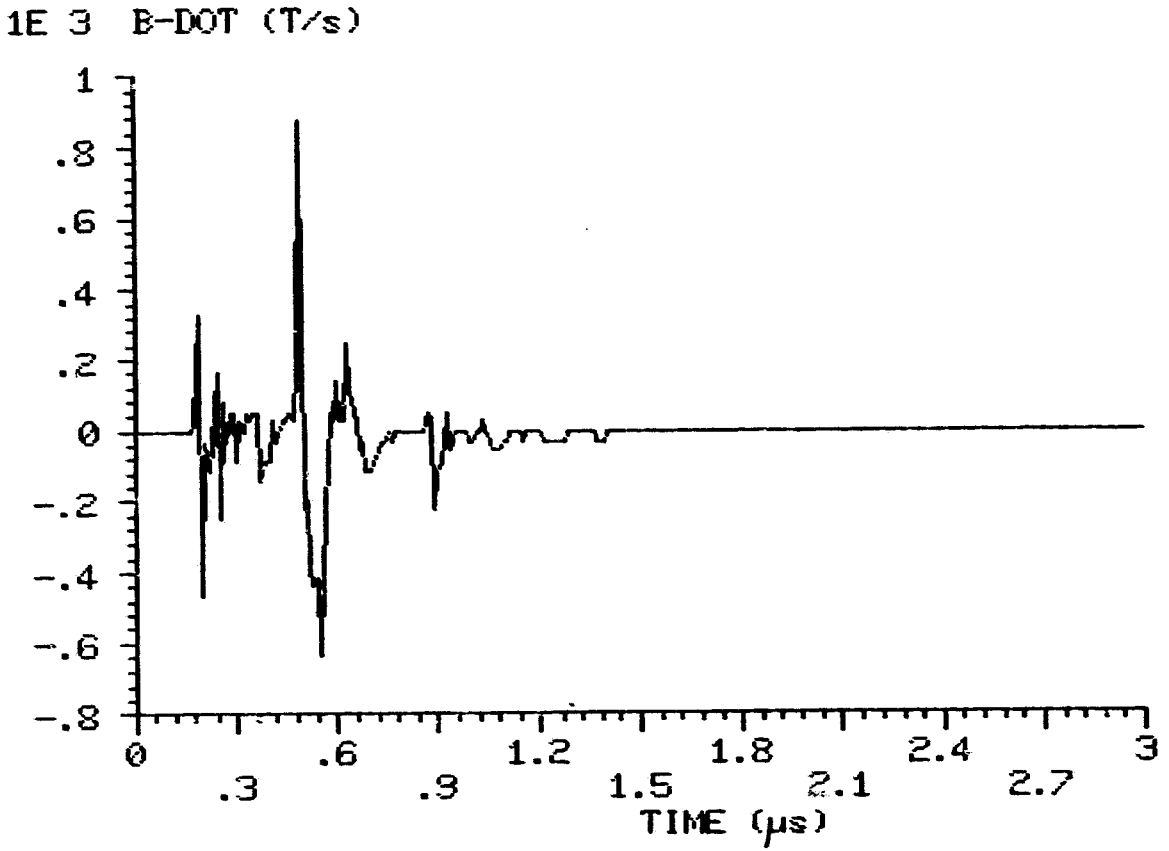

Fig. 11. B-dot waveform from strike 82-38-02.

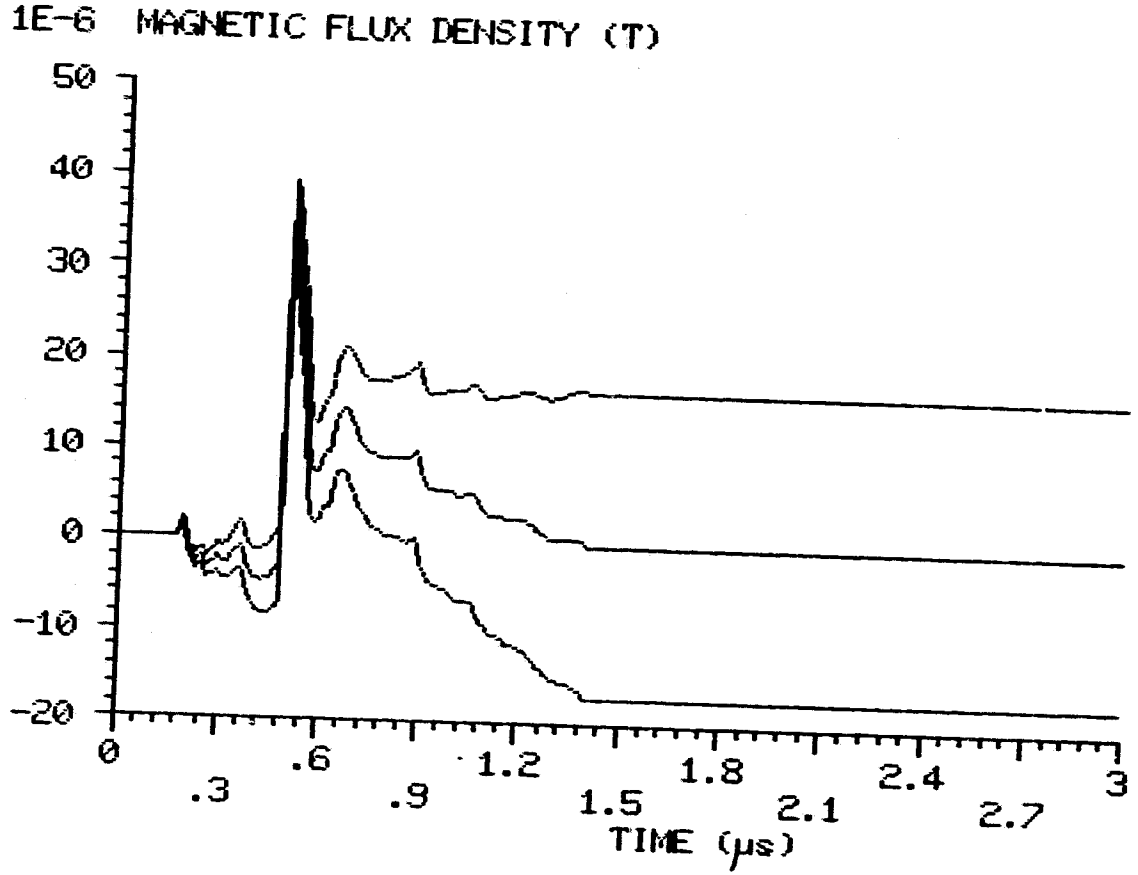

Fig. 12. B waveforms from time integral of B-dot in Fig. 11 (82-38-02).

I waveform is essentially a short pulse. Thus, since B and I are closely related, we assume in the present case that the final value of B should be zero, and we have multiplied the peak B-dot value by the factor, 4.27, which achieves this.

The picture that emerges from Figs. 10 and 12 taken together is that of a pulse of current which discharges the airplane. The situation is similar to the discharging of a capacitor through a resistor. If one assumes that the airplane is the capacitor, with a capacitance of approximately 500 pF (Appendix I), then, using $\tau = RC$, the 680 ns time constant gives a resistance of 1.4 kΩ for the circuit. The initial voltage, V, of the airplane can be estimated also. One way to do this is to estimate I from B and then make use of the fact that, at the instant when discharging begins, $V = I_{max}R$, where I_{max} is the maximum value of the current. To relate I and B we use the approximate result [6]

$$B \approx \mu_o I / (2\pi r) , \qquad (1)$$

where r is the effective radius of the airplane at the location of the B-dot sensor. Substituting 35 E-6 T for maximum B (from Fig. 12) and 3.0 m for r (from [6]), gives I_{max} = 530 A. Then V = 740 kV.

Changes in Waveform Spectra with Attachment-Point Location

As part of the laboratory scale-model tests described in [4], a model of the F-106B was connected to a pair of wires in four different ways to provide a variety of entry and exit points for

current pulses. The current entry and exit points are listed in Table II.

Table II. Wire Attachments on Model

Configuration	Entry	Exit
1	nose	engine exhaust
2	nose	port wingtip
3	starboard wingtip	port wingtip
4	belly	tail

For each attachment point configuration, transfer functions were computed relating the signals measured from small sensors mounted on the model to the entry-wire signal applied by a pulser. Fig. 13 shows the transfer functions for a B-dot sensor which was located and oriented like the B-dot sensor on the actual airplane shown in Fig. 1. As indicated on Fig. 13, the transfer functions are defined as $B_L(w) / V_{IN}(w)$, where $B_L(w)$ is the Fourier transform of the time-integral of the B-dot sensor output and $V_{IN}(w)$ is the transform of the pulser voltage. The frequency axes have been scaled to correspond to the actual plane. An inset along side each transfer function illustrates the model with wires to show the attachment locations.

The curves in Fig. 13 give information on the various resonant modes of the model that are excited by the current pulses. Some of the main characteristics of the curves are, first, for configurations 1 and 2, a peak at 7 MHz, second, for configuration 3, a dip at 13 MHz, and, third, for configuration 4,

TRANSFER FUNCTION $B_L(\omega)/V_{IN}(\omega)$ FOR F-106B MODEL

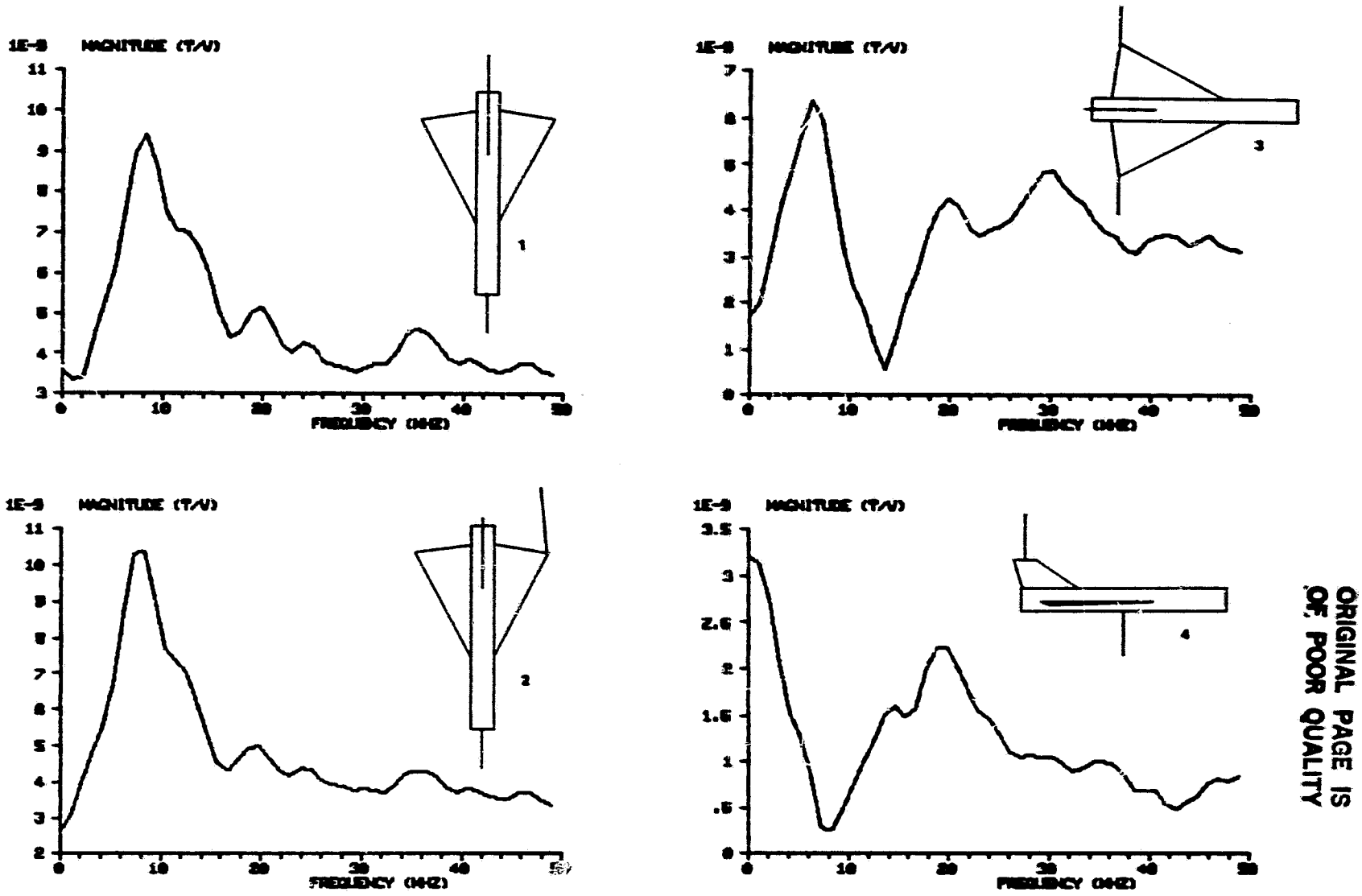

Fig. 13. Transfer functions of laboratory model for four wire-attachment configurations.

a peak at 20 MHz. Our interpretation of these characteristics is as follows: The 7 MHz resonance is the lowest one and has current flowing in the same direction along the whole length of the fuselage (like a half-wavelength dipole antenna). It is strongly excited in configurations 1 and 2. In configuration 4 the 7 MHz resonance is not excited because the midship attachment gives current to the front and back simultaneously; the spectrum peak is now at 20 MHz. In configuration 3 the 13 MHz resonance is conspicuously absent. Evidently it is not excited by the wingtip-to-wingtip input.

These results lead one to the conclusion that, if the attachment point locations were unknown, it would be possible to infer the locations based on an inspection of the transfer function. This idea can also be extended to the in-flight data.

Fast components in the lightning signatures can excite many of the aircraft resonances, and, in fact, in-flight B-dot waveforms often have spectra resembling the model transfer functions in Fig. 13, and it is easy to pick out the three cases, peak at 7 MHz, dip at 13 MHz, and peak at 20 MHz. Thus when we see a particular case in-flight, we infer the corresponding attachment. However, we cannot say <u>precisely</u> where the attachment points were located. For example, current entry at the noseboom or at the front of the fuselage would be expected to give about the same resonances. Also, notice that there is little difference in the transfer functions for configurations 1 and 2, where the exit point was changed. It is probably true in general that the location of the exit point does not affect the transfer

functions very much in the resonance region (f ≥ 7 MHz) because only a small amount of current is carried off by the wire. Furthermore, a nearby lightning flash, with no attachments at all, might produce spectra similar to those discussed here. Thus, at best, we infer only the likely region for current entry. Table III categorizes some in-flight results.

Table III. Inferred Attachments

Spectral Characteristic	Attachment (Entry)	In-Flight Examples
peak at 7 MHz	nose	82-38-02 (see [3]), 82-38-04, 82-40-04, 82-40-07, 82-42-06, 82-42-09
dip at 13 MHz	wingtip	80-38-04 (see [4])
peak at 20 MHz	mid-fuselage	80-38-01 (see [4]), 80-38-03A, 81-26-10, 82-37-04, 82-38-07B

III. RELATIONSHIPS AMONG THE WAVEFORMS IN STRIKE 84-17-01

The waveforms from the 1984 strike number 84-17-01 are similar to the 1982 aircraft-discharging waveforms already discussed, but they represent a more complete set, originating from eight rather than two external sensors. Several interesting comparisons can be made among the eight. Basically the event consisted of a several-hundred-ampere pulse at the noseboom, with a peak I-dot of 26.6 E+9 A/s (or 26.6 kA/μs). This is not a large current for lightning, but it produced a significant transient on an internal fuselage wire that went off-scale at 52 V. The signature of the current is a common one for strikes to the F-106B, consisting of a fast rise with some structure and a slow fall.

Data from 1984 is further improved because of the use of 8-bit, rather than 6-bit, transient recorders.

I and I-dot

The I sensor measuring noseboom current during 1984 was a shunt rather than a current transformer as in the past. On comparing the I waveform from 84-17-01 with the time-integrated I-dot waveform we find, in contrast to our similar comparison in Fig. 2, rather poor agreement. The waveforms are shown in Figs. 14 and 15, and several differences between them may be noted. The trailing edge of the pulse is almost completely missing in Fig. 15. This is due to insufficient dynamic range in the I-dot record. More specifically, the slope on the trailing edge in Fig. 14 varies from -8.7 E+8 A/s toward zero and thus is always less

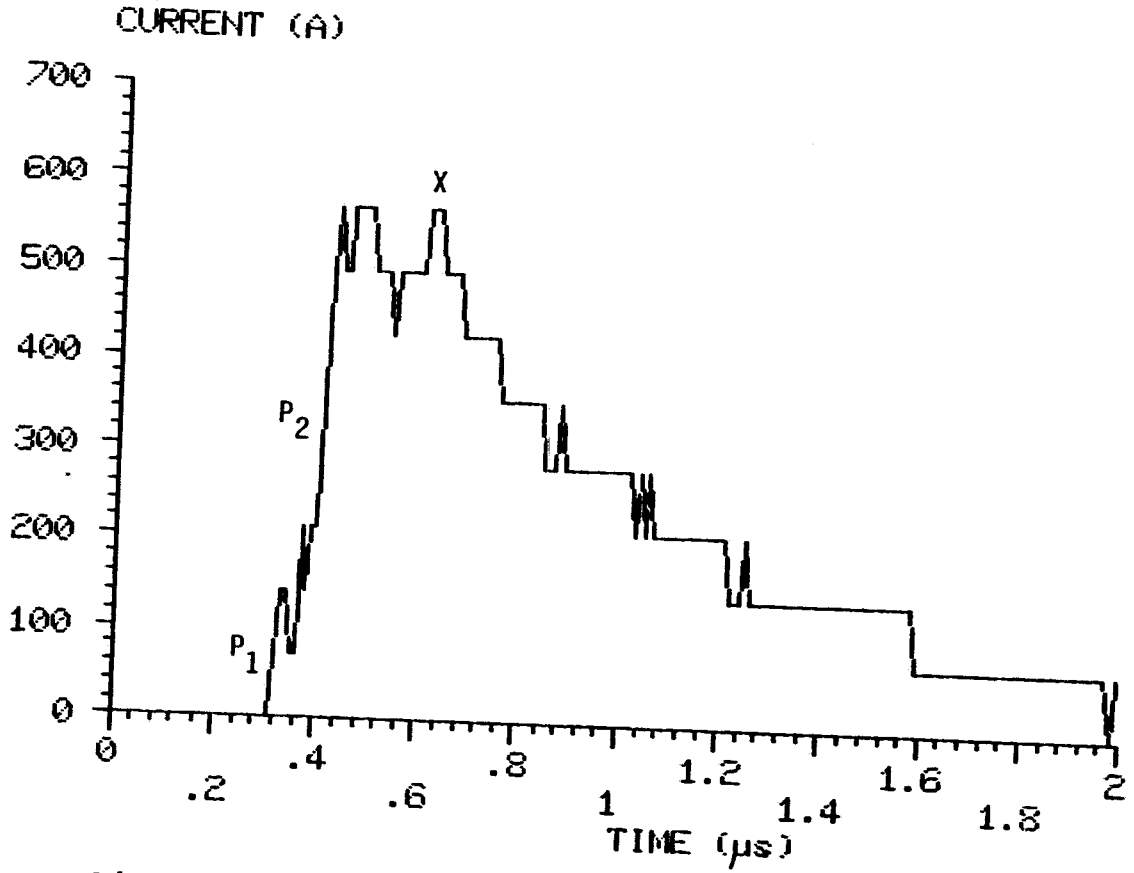

Fig. 14. Lightning noseboom current (I) waveform from shunt, strike 84-17-01. Sharp increases occur at points P_1 and P_2, and a continuous decline follows point X.

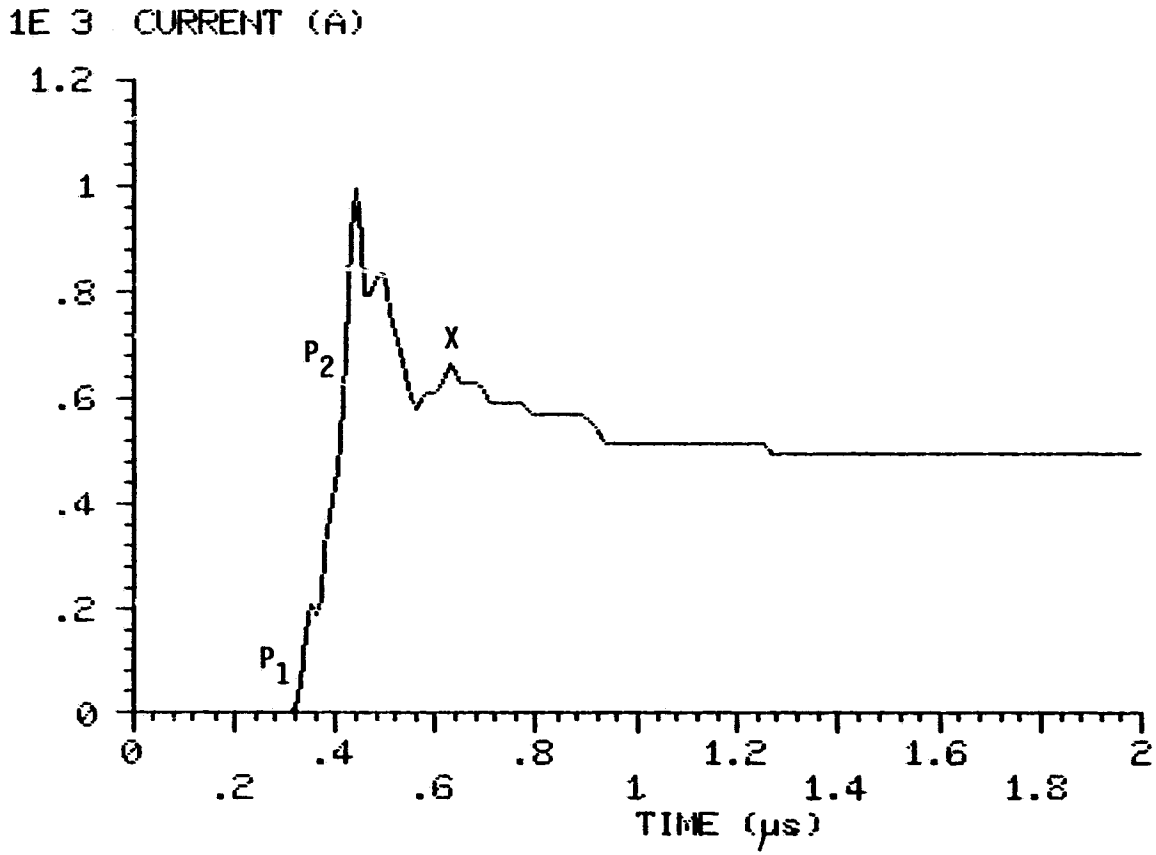

Fig. 15. Time integral of I-dot waveform from I-dot sensor for comparison with Fig. 14 (84-17-01).

than the first digitized level (below zero) in the I-dot record, -19 E+8 A/s. Other differences between the waveforms are that the peak value in Fig. 15 is much greater, and the curve descends more quickly following the peak than in Fig. 14. We expected that the amplitude of integrated I-dot would be greater than I, because the arrangement of sensors on the aircraft was such that some of the current bypassed the shunt but all of it went through the I-dot sensor; but the two waveforms were expected to have the same shape. The difference in shape may be due to quantization errors in I and I-dot or to some problem with the shunt. Further studies should be done to determine which of these is the case, because interpretation of the data is very difficult without knowledge of the true current waveform.

D-dot and I-dot

A very simple theoretical treatment (Appendix II) predicts that

$$\text{D-dot} \approx \text{I-dot} / (2\pi rc) \qquad (2)$$

for any fast disturbance, where r is the effective radius of the airplane at the location of the nose D-dot sensor. In order to see how closely the actual results follow the simple theory, we have taken the values 5.07 A/m^2 and 1.14 E+10 A/s from the first peaks (P_1) in D-dot and I-dot for substitution into this equation. The waveforms are shown in Figs. 16 and 17, respectively. Using r = 0.8 m, the result is 5.07 ≈ 7.56, which is not too bad.

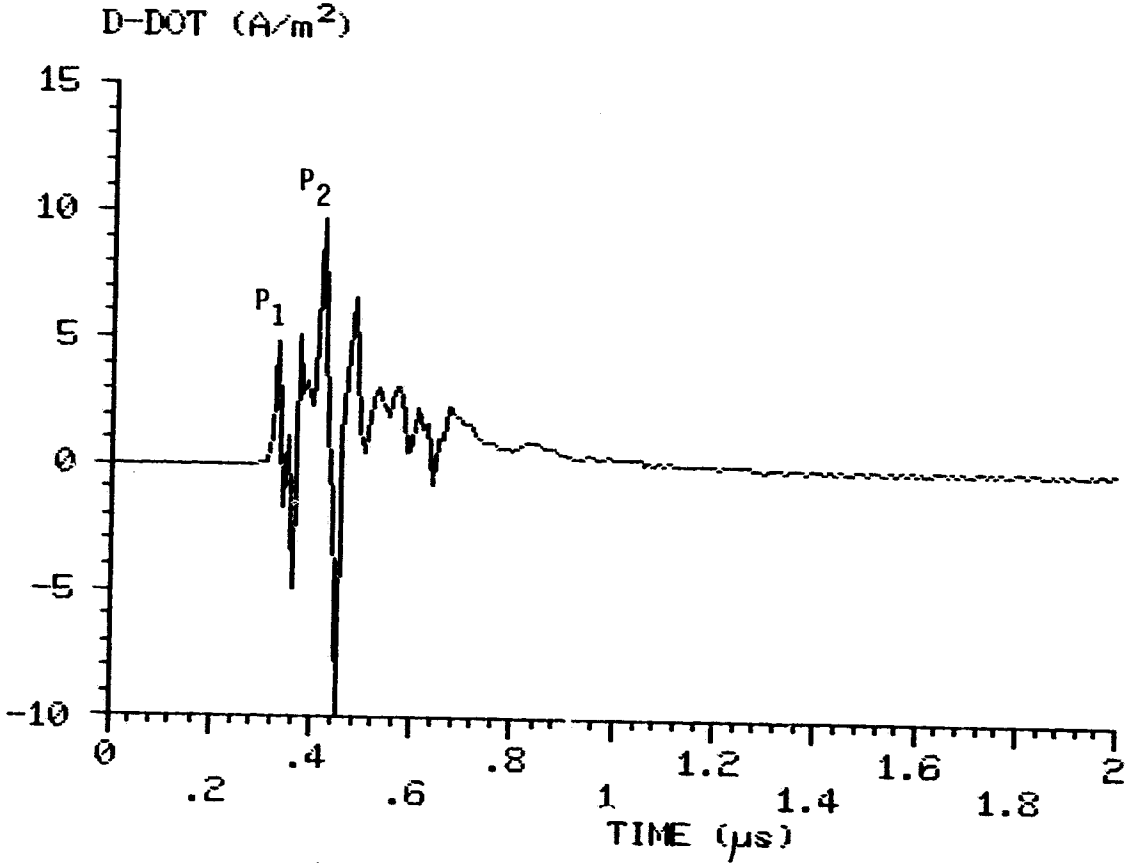

Fig. 16. D-dot waveform, strike 84-17-01.

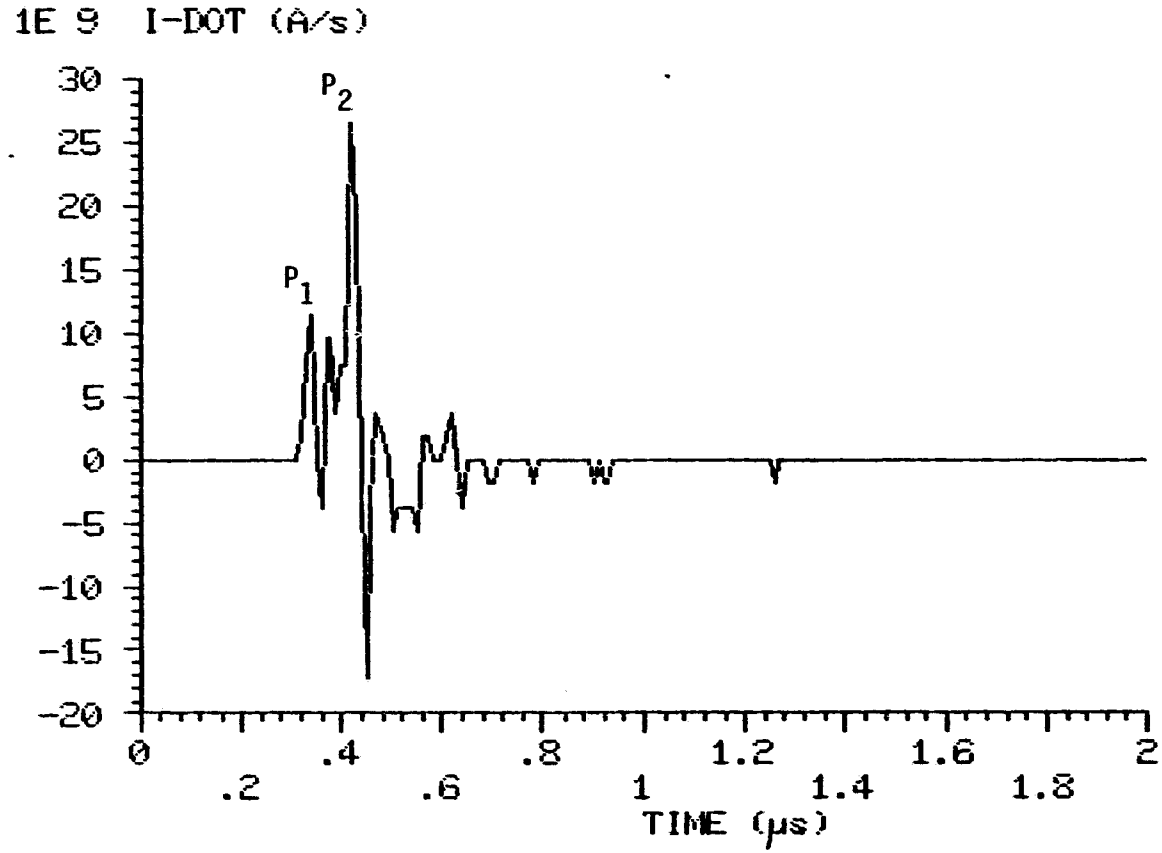

Fig. 17. I-dot waveform used to generate Fig. 15 (84-17-01).

B-dot and I-dot; B and I

The usefulness of Eq. 1 in Section II of this report may be checked by using the equation to determine the value of r for a number of different sets of B and I peak values. B-dot and I-dot peaks may also be used. For Eq. 1 to be useful, the values of r obtained should be nearly the same. Table IV shows some results. The first three entries in the table are taken from data appearing in [6].

Table IV. F-106B Effective Radius, r

Source of Data	Peaks Compared	r (m)
Langley gnd. test	B-dot, I-dot	4.1
INDCAL code	B-dot, I-dot	3.6
Texas Tech lab. model	B, I	3.0
84-17-01	B-dot, I-dot (first peaks)	2.7
84-17-01	B-dot, I-dot (largest peaks)	3.8
84-17-01	B, I (from shunt)	3.2
84-17-01	B, I (from I-dot)	5.7

The B-dot waveform and its time integral, B, used for the last four entries in Table IV are plotted in Figs. 18 and 19. All values of r in the table cluster together, lying between 2.7 and 4.1, except for the last one, at 5.7. There does not seem to be any obvious explanation for this large value. Possibilities appear to be, first, inaccurate data due to inadequate sampling

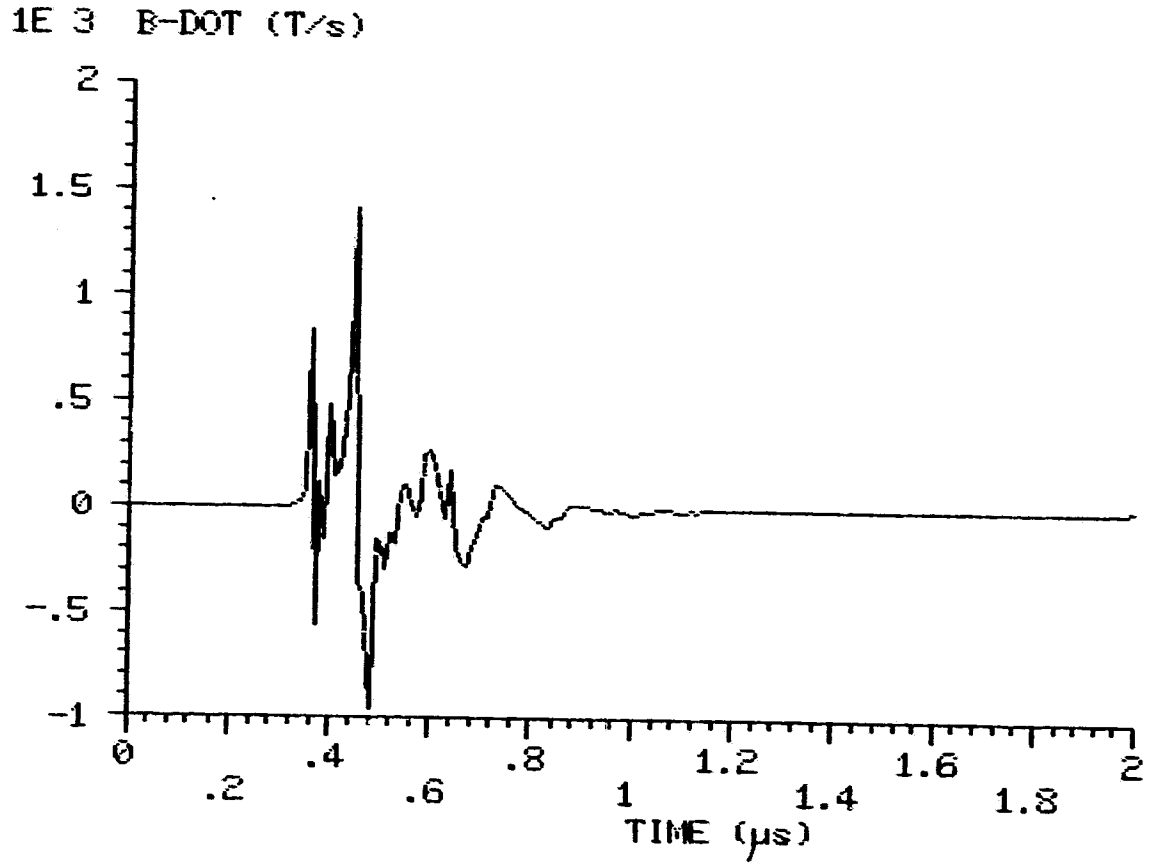

Fig. 18. B-dot waveform, strike 84-17-01.

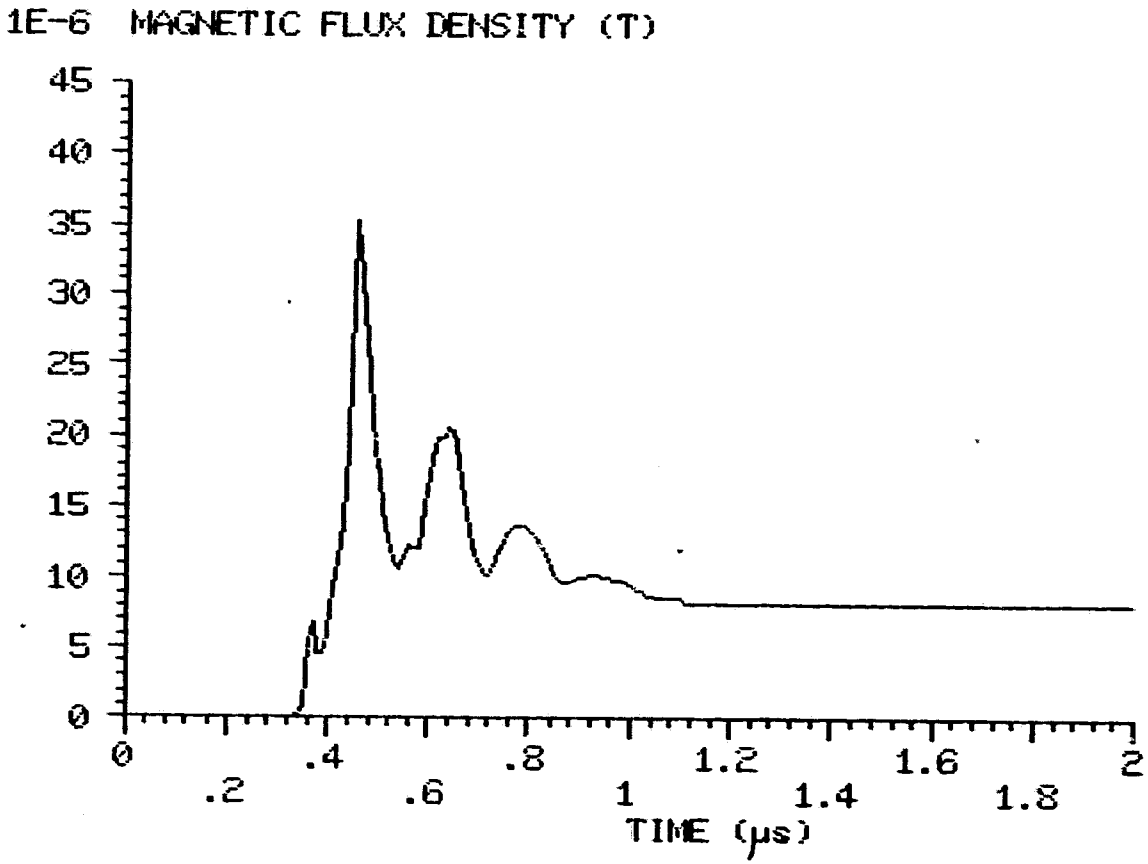

Fig. 19. Time integral of B-dot in Fig. 18 (84-17-01).

speed and, second, inaccuracies due to excessive spacing between amplitude quantization levels.

I and E

The integral of the nose D-dot signal in Fig. 16 leads to the E waveform of Fig. 20. This reveals aircraft discharging like that discussed above for the 1982 data. However, for 84-17-01 more complete data is available. In addition to the four sensors already described (Fig. 1), other sensors were used as follows: I on the tail, D-dot on the tail, D-dot under the port wing, and B-dot under the port wing for transverse currents. The tail I record consists of fluctuations between 0 and 71 A during the entire length of the transient recorder memory, 650 μs. 71 A is the first level above zero, and so the average current was, very roughly, 35 A. The polarity was such that electrons were flowing onto the airplane. We interpret this as a weak, continuing lightning-channel current which was <u>charging the airplane</u>. A large amount of corona would be expected on the airplane extremities during this charging phase. When the required conditions were met, a new channel formed from the noseboom, and the airplane was discharged. The development of the noseboom channel probably took place in step-wise fashion. This is suggested by the structure on the leading edge of the current pulse in Fig. 14. Two consecutive sharp rises in current are seen; they are labeled P_1 and P_2 in the figure. These sharp increases correspond to pulses in the I-dot waveform, and the pulses have been labeled with the same notation in Fig. 17. In

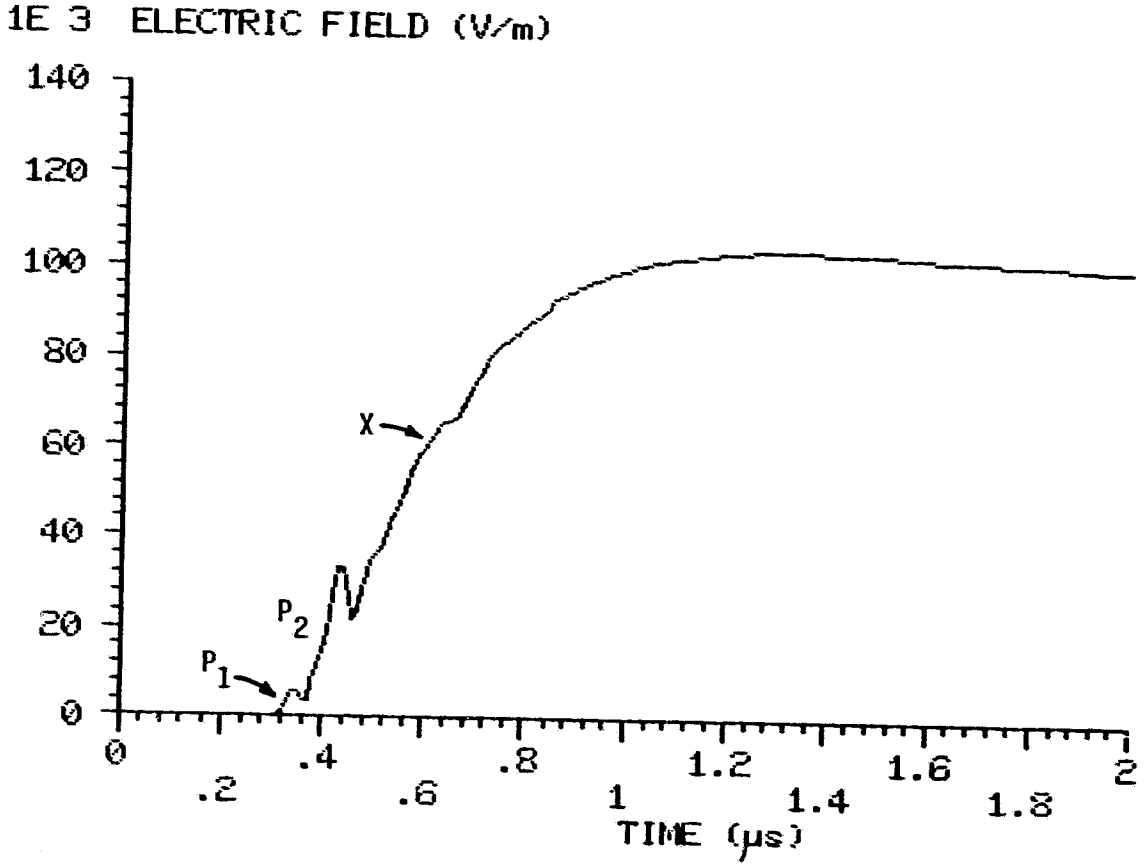

Fig. 20. E waveform from time integral of D-dot in Fig. 16 (84-17-01).

fact, the two events are also revealed in D-dot and E. See Figs. 16 and 20. The situation here is an example of a group of fast pulses like those analyzed earlier in this report in Fig. 7. We thus come to interpret these pulses as corresponding to the development, or connection, of a discharge channel. Once the peak current is reached in Fig. 14, there is a brief semi-flat spot, and then an exponential decay begins as the charge stored on the aircraft pours into the new channel. The exponential discharge is also seen in the E waveform of Fig. 20. Remember that, with this interpretation, the true zero of E would be at the top of the curve, not at the bottom.

A simplified equivalent circuit for this scenario is shown in Fig. 21. The airplane is represented by the capacitor, C. Charging current at the tail is supplied by the source I_C, and the channel at the noseboom is represented by the variable resistor. One imagines that the resistance of the resistor drops from a high value in step-wise fashion, producing the pulses P_1 and P_2, and reaches a value, R, for the discharge phase.

We have taken the beginning of the discharge phase to be at point X in Fig. 14. The time constant, τ, for the discharge (the time to fall to e^{-1}) is found from Fig. 14 to be 520 ns. With reference to the circuit in Fig. 21, a number of electrical parameters can now be computed. Using $\tau = RC$, the resistance, R, is found to be 1040 Ω. The voltage across the capacitor, C, and thus the airplane, after the channel has connected and the discharge begins is given simply by $V = - IR$. Taking I as the current at point X in Fig. 15, 665 A, gives V = - 692 kV. Here it

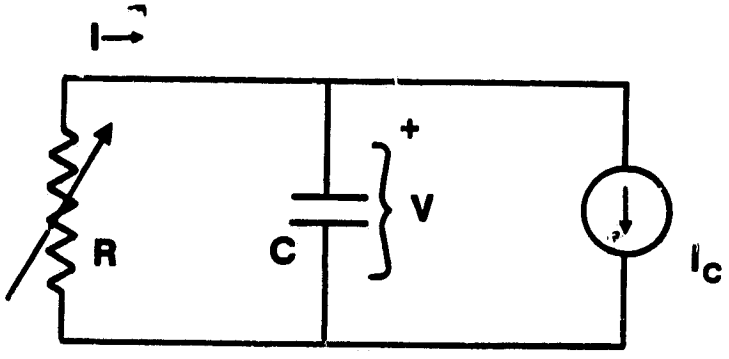

Fig. 21. Equivalent circuit for aircraft charging and discharging scenario applied to strike 84-17-01.

is better to use Fig. 15 than Fig. 14 because, as mentioned above, some fraction of the total current bypassed the sensor which was used to obtain Fig. 14. Next, the total energy, W, stored in the capacitor is given by $W = 1/2\ CV^2 = 120$ J. The peak pover delivered to the channel can also be found: $P = -IV = 4.60$ E+8 W, or 460 MW.

An alternative method for calculating the voltage and energy uses the charge, q, transferred from the capacitor. From Fig. 21 one sees that the capacitor current is the difference between the tail current (I_C) and the noseboom current (current through R). Integrating this difference gives q = - 298 E-6 C. To determine the charge, Q, on the capacitor at time X, q must be added to the charge remaining at the end of the pulse, which is given by $-CI_CR$ = - 18.2 E-6 C. Thus Q = - 316 E-6 C, and V = Q/C = - 632 kV. Then $W = 1/2\ CV^2 = 99.9$ J.

The two methods in the preceding paragraphs for calculating the energy give nearly the same results, and we conclude that W = 100 J. Note that our calculations apply to the discharge phase of the event; a quantitative analysis for the channel development phase, when the resistor in Fig. 21 is varying, has not yet been carried out.

A small but interesting effect, which we neglected, is the very slight drop in E after 1.3 μs in Fig. 20. This may be due to a late-time increase in the channel resistance, R. Another result from Fig. 20 is that the time constant for discharge of E is less than that for I in Fig. 14. This indicates the approximate nature of our understanding of this type of lightning event; future data

should help to provide a better understanding.

To put the values calculated above into perspective, we have compared the electrical discharge from the airplane to the discharge of a typical power-supply capacitor in an electronics package. The results are shown in Table V. The peak power, P, was calculated in both cases assuming a resistance of 1040 Ω.

Table V. Comparison of Discharges, Airplane and Capacitor

	C (μF)	V (V)	Q (μC)	W (J)	P (W)
Airplane	.0005	632,000	316	100	4.20 E+8
Capacitor	100	100	10,000	0.5	96.2

One can see from the values that C and Q are small for the airplane, but V is large. Thus the energy stored and the peak power delivered are large for the airplane.

IV. CONCLUSIONS

This report is concerned with the extraction of information from the in-flight data, and several basic types of information have been discussed. These are 1) the consistency and accuracy of the data recordings, 2) the electromagnetic characteristics of the lightning, and 3) the electromagnetic characteristics of the F-106B.

Data Consistency and Accuracy

Comparisons between I and the time-integral of I-dot showed good agreement in Fig. 2 (from 1982) but poor agreement in Figs. 14 and 15 (from 1984). Finding the reason for the lack of agreement in Figs. 14 and 15 will require the study of data from additional strikes.

The old I sensor distorted the lightning pulses because of its low-frequency cutoff behavior, making the pulses bipolar. See Figs. 4 and 5. We showed that we could correct for this distortion. Actually, there are only a few old waveforms that need to be processed in this way, but they are significant ones because they tie together the F-106B data with ground-based studies of other workers. These waveforms (Figs. 4 and 5) are similar, for example, to the lightning current waveforms that have been inferred by Weidman and Krider [7] from remote measurements of lightning fields.

Computer integration of the time derivative data, as in Figs. 10 and 12, can leave considerable uncertainty in the final value of the integrated waveform, due to the errors introduced by

quantizing the data. The new 8-bit transient recorders will help to alleviate this problem, but the gains of the recorders must always be carefully adjusted to make maximum use of the available dynamic range.

Characteristics of the Lightning

Fast pulses, like those marked with arrows in Fig. 6, are very prominent in the time-derivative data. They come in bunches of two to three and are among the fastest components ever observed in lightning fields. They may be associated with the development of leader channels on the noseboom, as illustrated in Fig. 9, where negative charge is carried off of the airplane. The time required for three pulses is typically in the range 100 to 700 ns.

By integrating D-dot waveforms like the one in Fig. 6, one discovers that there is an approximately exponential variation in D, and E, following the occurrence of the fast pulses. This is similar to the decay of the voltage of a capacitor as it discharges into a resistor. A possible interpretation of the overall event is that a channel is produced during the time of the pulses, and the charge on the aircraft dumps into this channel during the time of the exponential variation. In Figs. 14 and 20 the waveforms for E and simultaneous current, I, are given for one such event, strike 84-17-01. Values of various quantities for the exponential discharge phase are given in Tables I and V, where all values seem reasonable. In particular, in 84-17-01 it appears we have an event with an energy of 100 J, which is fairly potent.

If the RC-discharge idea for strike 84-17-01 is correct, the

necessary apparatus for an approximate simulation of this event on the ground is suggested by Fig. 21: A high-voltage power supply is connected to the tail of the aircraft through a large resistor to simulate the source, I_c. The aircraft is charged to - 650 kV and then allowed to spark over at the noseboom to a 1000 Ω resistor connected to ground.

Although Section III contains numerous comparisons between measured quantities, one ratio of quantities has thus far not been mentioned-- E / H. From Figs. 19 and 20 and using $B = \mu_0 H$ we find (max. E)/(max. H) = 3710 Ω. This value is ten times that of a free-space electromagnetic wave, indicating the importance of the electric field vis-a-vis the magnetic as earlier suggested by Baum [8].

Finally, the simple relationships between D-dot and I-dot in Eq. 2 and between B and I in Eq. 1 are only roughly correct for the lightning fields.

Characteristics of the F-106B

The double-hump signature shown in Fig. 8 is a characteristic of a nose-mounted D-dot sensor on the F-106B or other similar delta-wing aircraft subjected to a fast transient input at the nose. It is an example of the influence of aircraft shape on lightning waveforms.

Because of aircraft resonances, the spectral content of lightning signals from the B-dot sensor can be used to infer the locations of the lightning attachment points on the aircraft, as illustrated in Table III. This result is one benefit of

laboratory scale-model measurements (Fig. 13).

As a final comment, it is interesting that the time-derivative data reveals important short-time-scale information--fast lightning pulses and aircraft resonances and reflections (double hump)-- while by merely integrating, one gets data which emphasize a longer-time-scale picture, giving the overall discharge time and energy and suggesting the RC circuit interpretation.

APPENDIX I: CAPACITANCE OF F-106B

The capacitance between a circular disk of radius r and a sphere at infinity is given by $C_d = 8\epsilon_o r$. For a sphere rather than a disk, $C_s = 4\pi\epsilon_o r$. We approximate the capacitance of the F-106B to lie between that of a disk of radius 5.8 m and that of a sphere of the same radius. We obtain C_d = 410 pF and C_s = 645 pF, and thus for the airplane we take C = 500 pF.

APPENDIX II: RELATION BETWEEN D-DOT AND I-DOT

The simplest case for the propagation of an electromagnetic disturbance is one where the disturbance maintains the same shape as it travels and thus is given by f(z-vt). This would be the situation for a wave inside a uniform, lossless coaxial transmission line, for example. We will assume this is approximately correct for propagation of lightning disturbances along the noseboom and forward fuselage of the F-106B. For the propagation speed, v, we use c = 3.00 E+8 m/s.

We will let the z axis run through the noseboom and forward fuselage and take the fore-to-aft lightning current and surface charge to be approximately symmetrically distributed about this axis. The equation of conservation of charge can now be written in the form

$$\delta i/\delta z + \delta q/\delta t = 0 \quad ,$$

where i is current and q is surface charge per unit length in the axial direction. If i is a function of z-ct, then

$$\partial i/\partial z = - 1/c \; \partial i/\partial t \quad .$$

Charge conservation now becomes

$$\partial q/\partial t = 1/c \; \partial i/\partial t \quad .$$

If the fuselage is approximately circular with radius r, then the charge per unit area is $q/(2\pi r)$, and this is the same as the electric displacement, D. Thus, dividing the equation above by $2\pi r$, we find

$$D\text{-dot} = I\text{-dot}/ (2\pi rc) \quad ,$$

using the "-dot" notation employed in the body of this report.

REFERENCES

1. Wood, G. W. and T. F. Trost, "Electromagnetic Resonances of Cylinders and Aircraft Model with Resistive Wires," Air Force Weapons Laboratory Report AFWL-TR-84-90, Kirtland AFB, New Mexico, 1985.

2. Wen, C.-T. "Analysis of Lightning Transients on an Aircraft," M.S. Thesis, Texas Tech University, May, 1985.

3. Trost, T. F. et al. "Some Results and Limitations of Prony Analysis of In-Flight Lightning Data," Proc. Intl. Conf. on Lightning, Ft. Worth, Texas, 1983.

4. Turner, C. D. and T. F. Trost, "Laboratory Modeling and

Analysis of Aircraft-Lightning Interactions," N.A.S.A. CR 169455, 1982.

5. Hutzler, B. et al. "High Voltage Laboratory Tests and Lightning Phenomena," Proc. Intl. Conf. on Lightning, Paris, France, 1985.

6. Trost, T. F. and F. L. Pitts, "Analysis of Electromagnetic Fields on an F-106B Aircraft During Lightning Strikes," Proc. Intl. Conf. on Lightning, Oxford, England, 1982.

7. Weidman, C. D. and E. P. Krider "The Radiation Field Waveforms Produced by Intracloud Lightning Discharge Processes," J. Geophys. Research, vol. 84, pp. 3159-3164, 1979.

8. Baum, C. E. "Simulation of Electromagnetic Aspects of Lightning," Lightning Technology, NASA Conf. Pub. 2128, 1980.